Civil and Environmental Engineering
Vol. 21, Issue 2, 1292-1303, DOI: 10.2478/cee-2025-0095

BAYESIAN-OPTIMIZED FULLY CONNECTED NEURAL NETWORK FOR ENHANCED PREDICTION ACCURACY IN CONCRETE COMPRESSIVE STRENGTH ESTIMATION

Jiangyu XIONG[1], Zhengfeng MA[1,2,*], Haoyun YANG[1], Chen YANG[1], Jingyi CHEN[1]

[1] School of Civil and Transportation Engineering, Qinghai Minzu University, Xining, China
[2] College of Traffic & Transportation, Chongqing Jiaotong University, Chongqing, China
[*] corresponding author: 406149320@qq.com

Abstract

Concrete compressive strength serves as a critical quality control metric in construction engineering. Traditional empirical formulas and regression models struggle to capture multifactorial nonlinear relationships, while neural networks often exhibit hyperparameter sensitivity and overfitting issues. This study develops a Bayesian-optimized fully connected neural network (BO-FCNN) that employs Gaussian process surrogate modeling to dynamically identify optimal hyperparameters (e.g., learning rate, neuron count), enhancing generalization capability. Utilizing 1,015 experimental datasets from the UCI repository, feature selection integrated Pearson-Spearman correlation with random forest importance ranking. The optimized model achieved state-of-the-art performance: MSE = 21.0745 MPa^2, R^2 = 0.9080, MAE = 3.5028 MPa. Within the primary strength range (10–60 MPa), predictions showed strong agreement with experimental data, confirming the efficacy of Bayesian optimization in enhancing predictive accuracy. This establishes a robust computational framework for concrete strength prediction, enabling sustainable mix design optimization.

Keywords:

Bayesian optimization;
Fully connected neural networks;
Concrete compressive strength;
Strength prediction.

1 Introduction

As a fundamental construction material, global concrete consumption reached 40 billion tons in 2023 [1], with extensive applications in infrastructure including buildings, roads, and bridges. Compressive strength is a pivotal mechanical parameter throughout the project lifecycle, determining structural load-bearing capacity, influencing construction schedule control, and ensuring quality compliance during acceptance phases. In high-rise construction, insufficient strength delays formwork removal, extending schedules by ≥30% [2], while over-conservative designs increase material waste and carbon emissions. Concrete performance is governed by nonlinear coupling effects among critical factors: cement type [3], coarse aggregate gradation [4], admixture dosage [5], and fiber content [6]. These multidimensional interactions create complexities that challenge strength prediction.

Within sustainable building initiatives, eco-efficient concrete composites - notably fly ash-based concrete (FA-C) [7] and recycled aggregate concrete (RAC) [8] - show progressive annual adoption increases. These materials exhibit distinct multifactorial responses: FA-C displays exponential strength decay (40% reduction at 20% fly ash content) [9]. Predictive modeling reduces trial mix cycles by 50% [10] and ASTM C39 specimen requirements by 60%.

Conventional methods (empirical formulas, regression models [11], and non-destructive testing) face dual limitations: incapacity for nonlinear characterization and vulnerability to environmental interference, compromising construction quality control [12]. The Bolomey equation shows limited predictive capacity (R^2<0.78, RMSE=12 MPa) [13], while rebound hammer tests exhibit 15.8% error at -5 °C, requiring costly laboratory calibration [14]. Traditional formulas particularly fail to address multivariate nonlinear responses in advanced materials like FA-C and RAC, resulting in inefficient trial mix processes.

Machine learning addresses these challenges with unique advantages: 1) Support vector regression (SVR) leverages kernel functions to map features into high-dimensional spaces, achieving $R^2 = 0.89$ in fly ash content prediction [15]. 2) Ensemble models like random forest (RF) enhance prediction through multi-decision tree aggregation, attaining $R^2 = 0.91$ on recycled concrete datasets [7]. Limitations persist: single models are vulnerable to data noise, while ensemble models are sensitive to feature collinearity [16]. Although deep learning architectures (e.g., LSTM networks) effectively capture curing-age dependencies, their extensive data requirements limit small-scale experimental applications.

With machine learning advancements, neural networks have demonstrated measurable success in concrete strength prediction [17]. The fully connected neural network (FCNN) offers advantages through global feature interaction, nonparametric modeling, and stacked nonlinear activation layers [18]. This architecture effectively captures nonlinear correlations in basalt fiber concrete compositions [19], providing a structurally simple alternative to 1D convolutional approaches. Challenges include small-sample overfitting and high-dimensional training inefficiency [20]. Bayesian algorithms enhance robustness and generalization via dynamic weight constraints [21], modified loss functions [22], and adaptive hyperparameter tuning [23]. These methods achieve <0.6% error in excavation deformation prediction [21] and MSE = 3.86 in strength prediction [22]. The BO-FCNN framework integrates feature importance ranking for interpretability [24] and employs expected improvement (EI)-driven surrogate modeling to efficiently navigate hyperparameter space [25].

This study develops a Bayesian-optimized fully connected neural network (BO-FCNN) incorporating surrogate model-driven hyperparameter adaptation, which enhances generalization while maintaining low overfitting. Comparative analysis confirms BO-FCNN's superiority over benchmark models, establishing a robust solution for quality control and performance prediction in concrete engineering.

2 Model development methodology

2.1 FCNN

The fully connected neural network (FCNN) is a deep learning model based on multilayer nonlinear transformations. Its core architecture comprises an input layer, hidden layers, and an output layer. The input layer receives raw data, with each feature corresponding to an input neuron. Hidden layers perform layer-wise nonlinear mapping through weight matrices and activation functions. These typically consist of multiple fully connected layers where each neuron connects to all outputs from the preceding layer, enabling complex feature interactions through parametric transformations. The output layer uses a single linear neuron for direct target value mapping. Forward propagation executes sequential layer-wise computation from input to output layers through two core operations: linear transformation and nonlinear activation.

Input to the j-th hidden layer neuron [18]:

$$z_j^{(h)} = \sum_{i=1}^{n} w_{ji}^{(h)} x_i + b_j^{(h)}, \tag{1}$$

where:
x_i - input vector,
n - the number of input features,
$w_{ji}^{(h)}$ - the weight matrix from input to the hidden layer,
$b_j^{(h)}$ - the hidden layer bias.

Hidden layer output:

$$a_j^{(h)} = f(z_j^{(h)}), \tag{2}$$

where:
f - denotes the activation function. Common activation functions include ReLU, Sigmoid, and Tanh. ReLU mitigates the vanishing gradient problem by maintaining a constant derivative of 1 for positive inputs, thereby avoiding gradient attenuation caused by multiplicative chain rules in traditional Sigmoid/Tanh functions-particularly advantageous for deep networks. Additionally, ReLU requires only

comparison and max operations, making it computationally more efficient than the exponential calculations required by Sigmoid/Tanh functions [26].

Input to the k-th output layer neuron:

$$z_k^{(o)} = \sum_{j=1}^{m} w_{ki}^{(o)}\, a_j^{(h)} + b_k^{(o)}, \tag{3}$$

Final output:

$$y_k = g(z_k^{(o)}), \tag{4}$$

where:
g - the output layer activation function.

Mean Squared Error (MSE) loss:

$$E = \frac{1}{N}\sum_{i=1}^{N}(t_i - y_i)^2, \tag{5}$$

where:
t_i - denotes the true value,
y_i - the predicted value,
N - the number of samples.

Weight update via gradient descent:

$$w_{ij}^{new} = w_{ij}^{old} - \eta\frac{\partial E}{\partial w_{ij}}, \tag{6}$$

where:
η - the learning rate.

2.2 Bayesian optimization (BO)

Bayesian optimization (BO) is an efficient global methodology for black-box function optimization. It constructs probabilistic surrogate models of the objective function, iteratively updates posterior distributions using historical evaluation data, and guides optimal sampling point selection via acquisition functions—approximating global optima with minimal iterations. Gaussian process (GP) regression typically serves as the surrogate model, mathematically expressed as:

$$f(x) = gp(\mu(x),\ k(x, x')), \tag{7}$$

where:
$\mu(x)$ - denotes the mean function representing prior estimates of $f(x)$,
$\mathrm{k}(x, x')$ - the covariance function characterizing similarity between x and x'.

A commonly used squared exponential kernel is specified as:

$$k(\,x, x') = \sigma^2 exp(-\frac{\|x-x'\|^2}{2l^2}), \tag{8}$$

where:
σ - the signal variance,
l - length-scale parameters.

The most prevalent Expected Improvement (EI) acquisition function is formulated as:

$$EI(x) = E\left[max(f(x) - f(x^+),\ 0)\right], \tag{9}$$

where:
$\mathrm{f}(x^+)$ - the current optimal value observed.

2.3 BO-FCNN hybrid framework

The BO-FCNN framework integrates Bayesian optimization with a fully-connected neural network architecture, employing an automated hyperparameter tuning mechanism to significantly enhance the performance and stability of concrete strength prediction. This process initiates by: 1) initializing the

Bayesian optimizer. 2) defining the hyperparameter search space. Within an iterative loop constrained by maximum iteration count, the framework proposes new parameters by maximizing the expected improvement function, dynamically constructs FCNN topology, then evaluates performance metrics on the validation set. Following parameter recording, it updates the Gaussian process posterior distribution. Upon loop completion, the optimal hyperparameter combination is selected and retrains the final model using combined training and validation datasets, culminating in test set prediction generation through error distribution analysis-thereby establishing a closed-loop optimization system spanning initial space definition to predictive output. Figure 1 depicts the computational architecture of this hybrid framework.

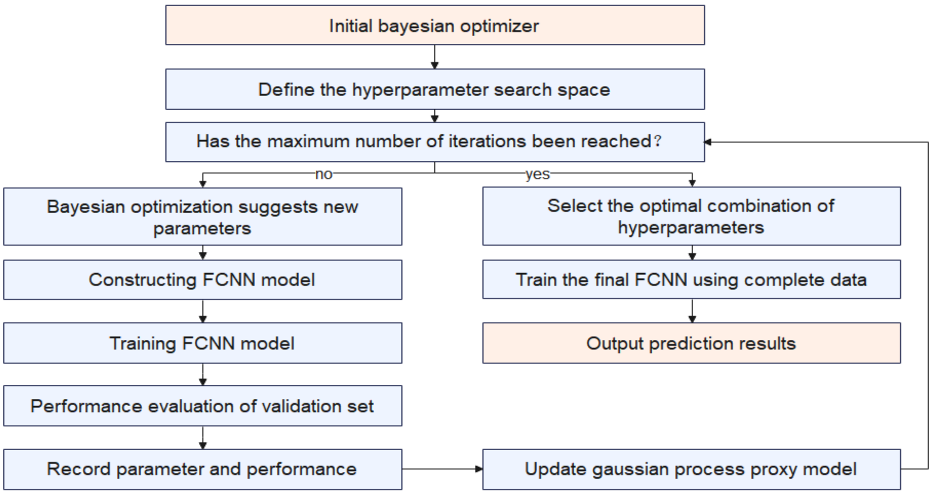

Fig. 1: Computational architecture of the Bayesian-Optimized FCNN (BO-FCNN).

2.4 Support vector regression (SVR)

Support vector regression (SVR), grounded in statistical learning theory, maps input data to a high-dimensional feature space via nonlinear transformation. It constructs an optimal regression hyperplane where deviations from all sample points remain within a preset threshold ε, using slack variables ξ and penalty factor C to accommodate errors:

$$\min_{\omega,b}\frac{1}{2}\|\omega\|^2 + C\sum_{i=1}^{m}(\xi_i + \xi_i^*), \tag{10}$$

where :
ω - the normal vector to the hyperplane,
b - the bias term,
C - the penalty factor controlling the penalty magnitude for samples exceeding the error threshold,
ξ_i, ξ_i^* - the slack variables handling sample errors outside the tolerance margin.

Subject to:

$$\begin{cases} y_i - (\omega\cdot\varphi(x_i) + b) \le \varepsilon + \xi_i, \\ (\omega\cdot\varphi(x_i) + b) - y_i \le \varepsilon + \xi_i^*, \\ \xi_i, \xi_i^* \ge 0 \end{cases} \tag{11}$$

The kernel function enables mapping of low-dimensional nonlinear problems to linearly separable high-dimensional spaces while avoiding explicit computation of high-dimensional coordinates, thus enhancing computational efficiency.

3 Experimental data preprocessing

The dataset comprises 1,030 concrete compressive strength records from the UCI Machine Learning Repository [27]. Collected through standardized cylindrical specimen testing across multiple institutions, these data ensure parameter consistency. Key parameters include mix proportions (water, cement, fly ash, slag, superplasticizer, coarse/fine aggregates) and curing age, with compressive strength ranging from 2.3 to 82.6 MPa. Selected specifications are documented in Table 1.

Table 1: Dataset characteristics of concrete compressive strength.

Cement[kg/m³]	Blast furnace slag [kg/m³]	Fly ash [kg/m³]	Water [kg/m³]	Super plasticizer [kg/m³]	Coarse Aggregate[kg/m³]	Fine Aggregate [kg/m³]	Age [day]	Concrete compressive strength [MPa]
540.0	0.0	0.0	162.0	2.5	1040.0	676.0	28	79.99
540.0	0.0	0.0	162.0	2.5	1055.0	676.0	28	61.89
332.5	142.5	0.0	228.0	0.0	932.0	594.0	270	40.27
332.5	142.5	0.0	228.0	0.0	932.0	594.0	365	41.05
198.6	132.4	0.0	192.0	0.0	978.4	825.5	360	44.30
266.0	114.0	0.0	228.0	0.0	932.0	670.0	90	47.03
...	...	...	...	...	...	...	...	...
260.9	100.5	78.3	200.6	8.6	864.5	761.5	28	32.40

3.1 Feature significance assessment

Feature selection employs dimensionality reduction to identify key predictors while eliminating redundant variables. This enhances model accuracy, reduces computational complexity, and maintains engineering rationality. Cross-validation across methodologies addresses feature importance variation. The Pearson correlation coefficient (Eq. 12) evaluates linear relationships under normal distribution assumptions, while Spearman's rank correlation (Eq. 13) assesses monotonic nonlinear associations robust to outliers.

$$r = \frac{\sum(x_i-\bar{x})(y_i-\bar{y})}{\sqrt{\sum(x_i-\bar{x})^2\sum(y_i-\bar{y})^2}}, \tag{12}$$

$$r_s = 1 - \frac{6\sum d_i^2}{n\,(n^2-1)}, \tag{13}$$

where:
$\bar{x}$ - denote feature values with mean x_i,
$\bar{y}$ - target values with mean y_i,
d_i - rank differences,
n - sample size.

Statistical significance is quantified using p-values. The null hypothesis ($p = 0$) indicates no significant correlation, while the alternative hypothesis ($p \neq 0$) suggests significant correlation. Lower p-values provide stronger evidence against $\alpha = 0.05$, with $p < 0.05$ as the significance threshold. Pearson and Spearman p-values are given in Equations 14 and 15, respectively.

$$p_1 = r\sqrt{\frac{n-2}{1-r^2}}, \tag{14}$$

$$p_2 = p_s\sqrt{n-1}, \tag{15}$$

Correlation coefficients and p-values are tabulated in Table 2. Retained features (cement, water, superplasticizer, curing age) show strong correlations ($|r|$, $|r_s| \geq 0.3$) and significance ($p < 0.05$), while weakly correlated features ($|r|$, $|r_s| < 0.3$) are preserved to capture synergistic effects. This strategy leverages the principle that feature combinations enhance predictive power even when individual features are weak predictors [28]. Figure 2 visualizes these feature-target correlations.

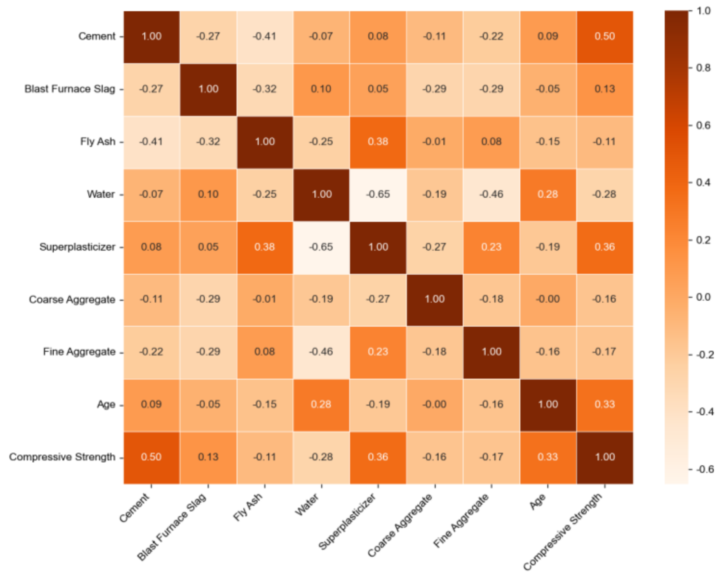

Fig. 2: Heatmap visualization of correlation coefficients.

Random forest (RF) enables automated feature selection through importance scoring. This ensemble method constructs multiple decision trees, quantifying feature importance via mean decrease impurity. This metric averages impurity reduction (Gini impurity or information entropy) across all splitting nodes. Table 2 shows curing age, cement content, and water-cement ratio as the highest importance features.

$$\text{Gini} = 1 - \sum_{j=1}^{m} p_j^2, \tag{16}$$

$$\text{Entropy} = -\sum_{j=1}^{m} p_j \log_2(p_j), \tag{17}$$

where:

p_i - the proportion of class m samples at node j,

m - the total number of classes.

Table 2: Multidimensional feature analysis.

Input Features	**Pearson Correlation [-]**	**Spearman Correlation Coefficient [-]**	**Pearson p-value [-]**	**Spearman p-value [-]**	**Importance score [-]**
Cement	0.4978	0.4776	1.32×10^{-65}	8.33×10^{-60}	0.3299
Blast furnace slag	0.1348	0.1625	1.41×10^{-05}	1.58×10^{-07}	0.0785
Fly ash	-0.1058	-0.0780	6.75×10^{-04}	1.23×10^{-02}	0.0170
Water	-0.2896	-0.3084	2.37×10^{-21}	3.96×10^{-24}	0.1067
Super plasticizer	0.3661	0.3476	5.08×10^{-34}	1.28×10^{-30}	0.0676
Coarse Aggregate	-0.1649	-0.1835	1.02×10^{-07}	2.97×10^{-09}	0.0273
Fine Aggregate	-0.1672	-0.1800	6.69×10^{-08}	5.99×10^{-09}	0.0375
Age	0.3289	0.5960	2.10×10^{-27}	4.47×10^{-100}	0.3354

3.2 Outlier detection and mitigation

Outlier treatment ensures data quality by addressing anomalies from measurement errors or operational deviations. Analysis of eight parameters revealed characteristic groups with significant strength variance ($p < 0.05$). Python-based IQR analysis (threshold multiplier = 1.5) identified 24 abnormal records across nine clusters. Mean imputation within clusters and removal of 15 irreparable records yielded 1,015 validated samples (Table 3).

Table 3: Outlier distribution across parameter clusters.

Cement [kg/m³]	Blast furnace slag [kg/m³]	Fly ash [kg/m³]	Water [kg/m³]	Super plasticizer [kg/m³]	Coarse Aggregate [kg/m³]	Fine Aggregate [kg/m³]	Age [day]	Concrete compressive strength [MPa]
359.0	19.0	141.0	154.0	10.9	942.0	801.0	28	62.94
359.0	19.0	141.0	154.0	10.9	942.0	801.0	28	59.49
359.0	19.0	141.0	154.0	10.9	942.0	801.0	3	25.12
359.0	19.0	141.0	154.0	10.9	942.0	801.0	3	23.64
359.0	19.0	141.0	154.0	10.9	942.0	801.0	7	35.75
359.0	19.0	141.0	154.0	10.9	942.0	801.0	7	38.61
359.0	19.0	141.0	154.0	10.9	942.0	801.0	56	68.75
359.0	19.0	141.0	154.0	10.9	942.0	801.0	56	66.78
362.6	189.0	0.0	164.9	11.6	944.7	755.8	91	79.30
362.6	189.0	0.0	164.9	11.6	944.7	755.8	91	79.30
362.6	189.0	0.0	164.9	11.6	944.7	755.8	91	79.30
362.6	189.0	0.0	164.9	11.6	944.7	755.8	91	79.30
446.0	24.0	79.0	162.0	11.6	967.0	712.0	3	35.36
446.0	24.0	79.0	162.0	11.6	967.0	712.0	3	25.02
446.0	24.0	79.0	162.0	11.6	967.0	712.0	3	23.35
446.0	24.0	79.0	162.0	11.6	967.0	712.0	7	52.01
446.0	24.0	79.0	162.0	11.6	967.0	712.0	7	38.02
446.0	24.0	79.0	162.0	11.6	967.0	712.0	7	39.30
446.0	24.0	79.0	162.0	11.6	967.0	712.0	56	61.07
446.0	24.0	79.0	162.0	11.6	967.0	712.0	56	56.14
446.0	24.0	79.0	162.0	11.6	967.0	712.0	56	55.25
446.0	24.0	79.0	162.0	11.6	967.0	712.0	28	57.03
446.0	24.0	79.0	162.0	11.6	967.0	712.0	28	44.42
446.0	24.0	79.0	162.0	11.6	967.0	712.0	28	51.02

3.3 Dataset normalization

Eight parameters served as model inputs with compressive strength as output. Table 4 details their statistical characteristics, revealing significant extremum and variance disparities (σ^2 range: 15.7-893.4), indicating non-uniform parameter distributions.

Table 4: Input feature parameters.

Parameter	Cement [kg/m³]	Blast furnace slag [kg/m³]	Fly ash [kg/m³]	Water [kg/m³]	Super plasticizer [kg/m³]	Coarse Aggregate [kg/m³]	Fine Aggregate [kg/m³]	Age [day]
Maximum value	540.00	359.40	200.10	247.00	32.20	1145.00	992.60	365.00
minimum value	102.00	0.00	0.00	121.75	0.00	801.00	594.00	1.00
mean value	279.32	74.16	53.81	181.88	6.13	973.17	774.01	45.79
variance	10811.35	7476.03	4108.66	455.42	35.76	6122.58	6482.79	4028.35

Min-max scaling normalized all features to [-1, 1] to mitigate magnitude disparity errors:

$$y_i = \frac{y - y_{min}}{y_{max} - y_{min}}, \tag{18}$$

where:
y_i - the normalized value,
y - the original value,
y_{max} , y_{min} - feature-specific extremums.

3.4 Data partitioning strategy

Common dataset partitioning ratios (Table 5) include 7:1.5:1.5 allocation. With 1,015 samples, this yields training (710), validation (152), and test sets (153). Per Hoeffding's inequality, the minimum training set size guaranteeing parameter estimation error ε < 5% at 95% confidence is:

$$n \geq \frac{\ln\left(\frac{2}{a}\right)}{2\varepsilon^2} = \frac{\ln\left(\frac{2}{0.05}\right)}{2\times 0.05^2} \approx 738, \tag{19}$$

where:
ε - estimation error,
a - significance level (0.05).

The 710-sample training set approximates this minimum (n = 738). The test set standard error is:

$$E = \sqrt{\frac{\sigma^2}{n_{test}}} = \sqrt{\frac{25}{153}} \approx 0.4, \tag{20}$$

This ensures compressive strength prediction errors within ±0.8 MPa at 95% confidence, meeting engineering accuracy requirements.

Table 5: Training-validation-test split configuration.

Proportional scheme	Applicable scenarios	advantage	disadvantage
8:1:1	Large-scale datasets (N > 100,000 samples)	Optimal training data utilization through stratified sampling	Limited validation data induces instability in hyperparameter optimization
7:1.5:1.5	High-complexity architectures	Enhanced applicability to high-dimensional hyperparameter spaces	Training data scarcity risks compromising model generalizability
6:2:2	Small-sample regimes (N < 1,000 samples)	Statistically robust error estimation	Risk of model underfitting due to insufficient learning capacity
5:3:2	Exploratory phase involving feature selection/engineering	Recommended for benchmarking studies requiring cross-validation	Critical insufficiency of training samples for convergence

4 Model performance evaluation

Using a 7:1.5:1.5 ratio, 1,015 samples were partitioned into training (710), validation (152), and test (153) sets. Performance was quantified using R^2, MSE, RMSE, and MAE (Equations 21-24). An R^2 approaching 1 indicates superior fit, while MSE disproportionately penalizes large errors. RMSE provides dimensionally homogeneous results, enhancing interpretability, whereas MAE remains robust to outliers.

Implemented in Python 3.8, we conducted real-time tracking of mean squared error (MSE) loss variations across learning rates. The initial search range spanned [1×10^{-6}, 1]. Through iterative range reduction at 10% per iteration, we refined the search to the optimal sub-interval [1×10^{-5}, 1×10^{-1}]. A learning rate of 1×10^{-5} exhibited sluggish convergence, indicating potential convergence to local minima and establishing the lower bound. Conversely, a learning rate of 1×10^{-1} induced severe oscillations, suggesting possible gradient explosion and defining the upper bound. Figure 3 illustrates these loss variations across learning rates. Neural networks with adequate hidden neurons can approximate any continuous function. Our artificial neural network (ANN) architecture, with hidden-layer configuration determined empirically, successfully modeled nonlinear relationships in 10-dimensional input spaces [29]. This demonstrates that moderate-to-large neuron counts (16-256) generally satisfy complex nonlinear modeling requirements, justifying our selection of 16-256 hidden units. After 20 optimization iterations, the BO-FCNN model achieved optimal hyperparameter configuration on the validation set, yielding peak performance metrics on the test set: R^2 = 0.9080, RMSE = 4.5907 MPa, MSE = 21.0745 MPa^2, and MAE = 3.5028 MPa (Figure 4).

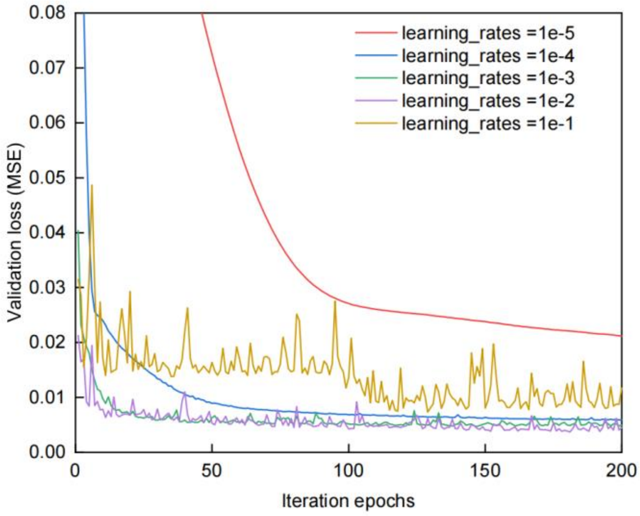

Fig. 3: Loss variation across learning rates.

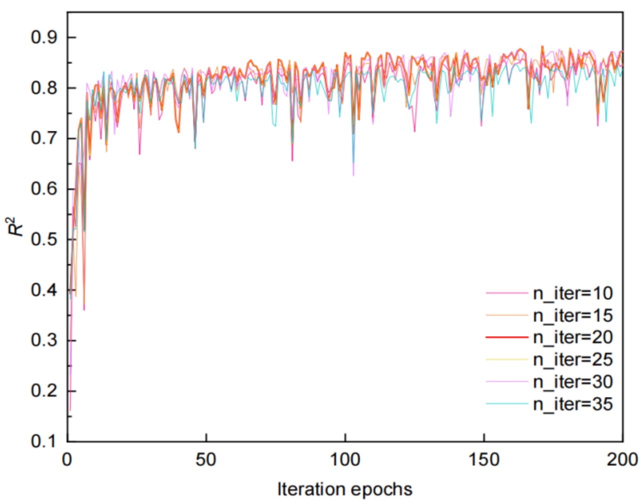

Fig. 4: Convergence behavior of Bayesian hyperparameter optimization.

Using Python 3.8, we implemented fully connected neural network (FCNN) and support vector regression (SVR) frameworks with identical input features. The FCNN architecture employed two hidden layers with 16-256 neurons and ReLU activation, achieving optimal performance (R^2 = 0.8246, RMSE = 6.3399 MPa, MAE = 4.8108 MPa). For SVR implementation, a radial basis function (RBF) kernel modeled nonlinear relationships. Concrete strength prediction experiments [30] identified C=100 as the optimal regularization parameter, yielding R^2 = 0.8792, RMSE = 5.2616 MPa, and MAE = 3.9809 MPa.

$$R^2 = 1 - \frac{\sum_{i=1}^{n} (X_i - Y_i)^2}{\sum_{i=1}^{n} (X_i - \bar{X})^2}, \tag{21}$$

$$\mathrm{MSE} = \frac{1}{n}\sum_{i=1}^{n} (y_i - y^*)^2, \tag{22}$$

$$\mathrm{RMSE} = \sqrt{\frac{1}{n}\sum_{i=1}^{n}(y_i - y^*)^2}, \tag{23}$$

$$\mathrm{MAE}=\frac{1}{n}\sum_{i=1}^{n}\left|y_i - y^*\right|, \tag{24}$$

where:
y_i - true value,
y^* - predicted value,
$\overline{X}$ - sample mean,
n - sample size.

Table 6: Cross-Model Performance Benchmarking.

Model type	MSE/MPa^2	R^2 [-]	RMSE/MPa [-]	MAE/MPa [-]
SVR	27.6844	0.8792	5.2616	3.9809
FCNN	40.1943	0.8246	6.3399	4.8108
FCNN+BO	21.0745	0.9080	4.5907	3.5028

Figure 5 demonstrates BO-FCNN's superior accuracy within the 10–60 MPa range, while Figure 6 compares relative error distributions across the three modeling approaches. Prediction points cluster closer to the ideal fit line, confirming enhanced precision through Bayesian optimization.

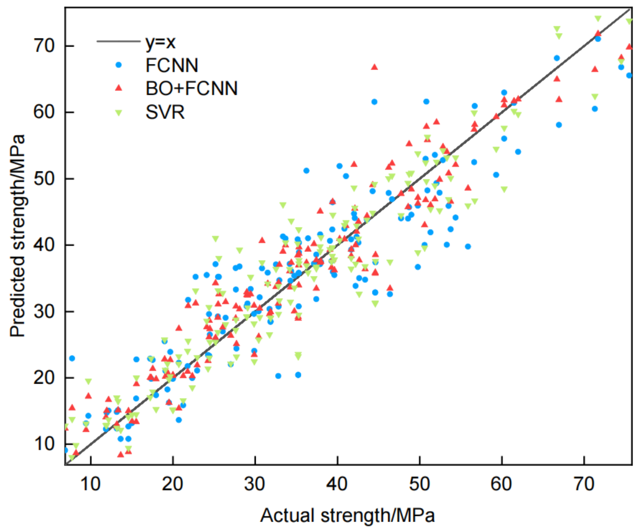

Fig. 5: Predictive accuracy metrics across modeling frameworks.

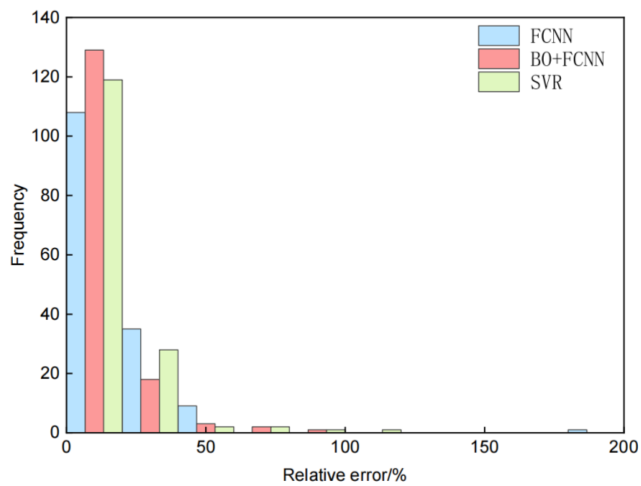

Fig. 6: Relative error distribution histograms.

5 Conclusion

This study addresses multifactorial nonlinear prediction challenges in concrete compressive strength by developing a Bayesian-optimized fully connected neural network (BO-FCNN). Feature importance analysis identified cement content, water-cement ratio, superplasticizer dosage, and curing age as critical input parameters. Gaussian process (GP) surrogate modeling coupled with expected improvement (EI) acquisition achieved hyperparameter self-adaptation, resolving empirical tuning dependency and small-sample overfitting in traditional networks. Experimental results demonstrate BO-FCNN's superiority: 47.5% and 23.9% lower MSE than FCNN and SVR respectively, 10.1% and 3.2% higher R^2 values, and 25.1% and 9.4% lower MAE values. These findings substantiate Bayesian optimization's generalization advantages. The methodology establishes a robust framework for concrete mix optimization and real-time strength assessment, while future work should explore multi-algorithm integration and multi-objective optimization for complex engineering applications.

Acknowledgements

The authors acknowledge the 2024 Kunlun Talent Program for High-End Innovative and Entrepreneurial Talents of Qinghai Province (QHKLYC-GDCXCY-2024-102), the 2024 Graduate Innovation Project of Qinghai Minzu University (66M2024026), and the 2023 University-Level Planning Project of Qinghai Minzu University (23GH10) for supporting this research.

References

[1] SCRIVENER, K.L. – JOHN, V.M. – GARTNER, E.M.: Eco-Efficient Cements: Potential Economically Viable Solution for a Low-CO_2 Cement-Based Materials Industry. Cement and concrete Research, Vol. 114, 2018, pp. 2–6.

[2] LATIF, S.D.: Concrete Compressive Strength Prediction Modeling Utilizing Deep Learning Long Short-Term Memory Algorithm for a Sustainable Environment. Environmental Science and Pollution Research, Vol. 28, 2021, pp. 30294–30302.

[3] NAGROCKIENE, D. – PUNDIENĖ, I. – KICAITE, A.: The Effect of Cement Type and Plasticizer Addition on Concrete Properties. Construction and building materials, Vol. 45, 2013, pp. 324–331.

[4] BADISSI, A.B. – BEROUAL, A. – BENTALHA, M.: Coarse Aggregate Grading Effect on the Correlation Between Compressive and Flexural Strengths of Concrete. Civil and Environmental Engineering, Vol. 20, Iss. 2, 2024, pp. 1221–1245.

[5] BROOKS, J.J. – JOHARI, M.M. – MAZLOOM, M.: Effect of Admixtures on the Setting Times of High-Strength Concrete. Cement and concrete Composite, Vol. 22, 2000, pp. 293–301.

[6] KAREM, S.T. – AL-ASADI, A.K.: Impact of Various Types of Fibres on the Mechanical Properties of Lightweight Concrete. Civil and Environmental Engineering, Vol. 20, Iss. 2, 2024, pp. 1255–1266.

[7] SHI, X. – DING, D. – SONG, H. et al.: Machine Learning-Based Strength Prediction of Fly Ash-Based Geopolymer Concrete. Industrial Construction, Vol. 1, 2025, pp. 1–12, http://kns.cnki.net/kcms/detail/11.2068.TU.20250102.1011.003.html.

[8] GAO, W.: Compressive Strength Prediction of Recycled Aggregate Concrete Using Deep Learning. Concrete, Vol. 11, 2018, pp. 58–61, 70.

[9] ZHENG, L.: Performance and Compressive Strength Prediction Model of Concrete with Composite Mineral Admixtures. Ph.D. Thesis, Zhejiang University, Hangzhou, China, 2012.

[10] GUAN, M.: Water-Cement Ratio Determination of Fresh Concrete and Compressive Strength Prediction. Master's Thesis, Qingdao University of Technology, Qingdao, China, 2021, DOI: 10.27263/d.cnki.gqudc.2021.000389.

[11] WU, X. – LIU, P. – CHEN, H. et al.: Random Forest-Based Compressive Strength Prediction of High-Performance Concrete. Concrete, Vol. 1, 2022, pp. 17–20.

[12] LUO, G. – HONG, C. – CHENG, Z. et al.: BP and GA-BP Neural Networks for Concrete Compressive Strength Prediction. Concrete, Vol. 3, 2023, pp. 37–41.

[13] CHOPRA, P. – SHARMA, R.K. – KUMAR, M. – CHOPRA, T.: Comparison of Machine Learning Techniques for the Prediction of Compressive Strength of Concrete. Advances in Civil Engineering, Vol. 2018, 2018, Art. ID 5481705.

[14] ZHANG, R. – YAN, H. – ZHANG, J. et al.: Variation Law and Prediction Model of Concrete Compressive Strength at −5 °C. J. Journal of Shenyang Jianzhu University (Natural Science Edition), Vol. 38, 2022, pp. 323–330.

[15] ZHANG, J.S. – GUO, G.: Reweighted Robust Support Vector Regression Method. Journal of Computer Science, Vol. 28, 2005, pp. 117–177.

[16] ERDAL, H. – ERDAL, M. – SIMSEK, O. – ERDAL, H.I.: Prediction of Concrete Compressive Strength Using Non-Destructive Test Results. Computers and Concrete, Vol. 21, 2018, pp. 407–

417.
[17] KASPERKIEWICZ, J. – RACZ, J. – DUBRAWSKI, A.: HPC Strength Prediction Using Artificial Neural Network. Journal of Computing in Civil Engineering, Vol. 9, 1995, pp. 279–284.
[18] XIE, H. – WU, M.: Pedagogical Exploration from Fully Connected to Convolutional Neural Networks. Fujian Computer, Vol. 36, 2020, DOI: 10.16707/j.cnki.fjpc.2020.07.040.
[19] LI, H.: Machine Learning-Based Compressive Strength Prediction Algorithm for Basalt Fiber Reinforced Concrete. Master's Thesis, Anhui University, Hefei, China, 2023, DOI: 10.26917/d.cnki.ganhu.2023.000755.
[20] XU, J. – FENG, Q. – YANG, S.: Application of Fuzzy System Method in Non-Destructive Testing for Concrete Compressive Strength Prediction. Engineering Mechanics, Vol. 6, 2007, pp. 104–110.
[21] YUE, J. – ZHONG, H. – GU, L. et al.: Application of Bayesian Regularized Neural Network in Deep Excavation Deformation Prediction. Journal of Henan University (Natural Science Edition), Vol. 52, 2022, pp. 200–209, DOI: 10.15991/j.cnki. 411100.2022.02.004.
[22] CHEN, H. – LONG, W. – LI, X. et al.: BP Neural Network-Based Compressive Strength Prediction of Fly Ash Concrete. Building Structures, Vol. 51, 2021, pp. 1041–1045.
[23] NIU, C. – LI, S. – HU, J. et al.: Machine Learning Applications in Materials Informatics. Materials Review, Vol. 34, 2020, pp. 23100–23108.
[24] KANG, L. – MI, X. – WANG, H. et al.: Research Progress of Artificial Neural Networks in Materials Science. Mater. Materials Review, Vol. 34, 2020, pp. 21172–21179.
[25] ZHANG, X. – DAI, C. – LI, W. et al.: TPE-XGBoost Based Compressive Strength Prediction Model for Recycled Coarse Aggregate Concrete. Journal of Building Science and Engineering, Vol. 41, 2024, pp. 100–110, DOI: 10.19815/j.jace. 2022.10013.
[26] BKA, M.A. – NGAMKHANONG, C. – WU, Y. – KAEWUNRUEN, S.: Recycled Aggregates Concrete Compressive Strength Prediction Using Artificial Neural Networks. Infrastructures, Vol. 6, Iss. 2, 2021, pp. 17.
[27] CHOU, J.S. – CHIU, C.K. – FARFOURA, M. – AL-TAHARWA, I.: Optimizing the Prediction Accuracy of Concrete Compressive Strength Based on a Comparison of Data-Mining Techniques. Journal of Computing in Civil Engineering, Vol. 25, 2011, pp. 242–253.
[28] ZHOU, J.F. – ZENG, X.H. – XIE, Y.J. et al.: Compressive Strength Prediction of Concrete Based on HEMNG Model. Journal of Railway Science and Engineering, Vol. 22, Iss. 2, 2025, pp. 875–886, DOI: 10.19713/j.cnki. 43-1423/u. T20240592.
[29] AKBARI, M. – JAFARI DELIGANI, V.: Data Driven Models for Compressive Strength Prediction of Concrete at High Temperatures. Frontiers of Structural and Civil Engineering, Vol. 14, Iss. 2, 2020, pp. 311–321.
[30] DEROUSSEAU, M.A. – LAFTCHIEV, E. – KASPRZYK, J.R. – RAJAGOPALAN, B. – SRUBAR III, W.V.: A comparison of machine learning methods for predicting the compressive strength of field-placed concrete. Construction and Building Materials, Vol. 228, 2019, Art. ID 116661.